Comparison of geophone and seismometer for regional-scale induced seismicity monitoring

Xinding Fang[*1,2], Siwei Li[1], and Tianrun Chen[1]*
[1]*SensorEra Inc, Houston, TX;* [2]*Department of Earth and Atmospheric Sciences, University of Houston, TX.*

Summary
This study investigates whether standard 5 Hz geophones can effectively replace broadband seismometers for regional-scale induced seismicity monitoring when their instrument responses are properly corrected. Although geophones are traditionally used for high-frequency applications such as active seismic surveys and microseismic monitoring, recent studies suggest that their frequency response can be extended to lower frequencies through deconvolution. We conduct a one-year comparative study using collocated 5 Hz geophone and broadband seismometer in Texas to evaluate the accuracy of event detection, waveform consistency, and source parameter estimation across a wide magnitude and distance range (up to ~300 km). The results show that, after instrument response correction, geophones can reliably record seismic signals down to approximately 0.2 Hz, and can be extended to ~0.1 Hz for regional-scale monitoring within ~100 km. The waveform cross-correlation coefficients exceed 0.85 for events with magnitudes ranging from M0.4 to M3.3 within a 30km radius and reach above 0.9 for events of M3 and greater within a 300km distance, provided that the signal-to-noise ratio exceeds 2. This study demonstrates that 5 Hz geophones, when properly calibrated and response-corrected, can achieve comparable detectability and accuracy to broadband seismometers for induced seismic monitoring, even for an event up to magnitude M5.4-the largest event recorded during the study period.

Introduction
Seismic monitoring plays a critical role in understanding both natural and induced seismicity, particularly in regions where human activities such as wastewater injection, hydraulic fracturing, and CO_2 sequestration alter subsurface stress conditions. Reliable monitoring systems are essential not only for detecting and characterizing seismic events but also for supporting risk assessment and regulatory compliance.

Traditionally, broadband seismometers have been the preferred choice for regional and local seismic networks because they can accurately record signals over a wide frequency range—from fractions of a hertz to tens of hertz—capturing the full spectral content of earthquakes, including long-period motions. In contrast, industry geophones, with typical natural frequencies of 4.5 Hz to 10 Hz, are designed primarily for high-frequency applications such as reflection seismology and microseismic monitoring. Their limited low-frequency response has historically precluded their use in regional-scale seismicity monitoring.

However, several studies have shown that geophones can, in fact, record meaningful low-frequency signals beyond their nominal natural frequency (Besedina et al., 2020; Hall et al., 2012; Rasmussen, 2019; Zou et al., 2010). Yenier et al. (2016) compared seismic data recorded by geophones and broadband seismometers and found that geophone-based magnitude estimates were systematically lower due to diminished low-frequency sensitivity—though their analysis did not include instrument response correction. When the geophone response is properly deconvolved, the amplitude and phase characteristics can be accurately restored across a wider frequency band, thereby enabling the recovery of low-frequency content well below the geophone's natural frequency.

This correction can be achieved through two approaches: (1) analog compensation using a frequency-dependent amplifier integrated into the acquisition circuitry, or (2) digital post-processing via deconvolution of the instrument response. The latter method offers greater flexibility and can be implemented retrospectively, allowing sensor-specific calibration to further enhance accuracy.

Given the substantially lower cost and ruggedness of geophones compared to broadband seismometers, it is of practical and economic interest to assess whether geophones can serve as a viable alternative for induced seismic monitoring networks—especially in regions requiring dense station spacing.

In this study, we conduct a detailed comparison of seismicity data recorded over one year by a collocated broadband seismometer and a 5 Hz industry-standard geophone, both deployed in West Texas. Our objectives are threefold: (1) To determine whether cost-effective 5 Hz geophones can reliably replace broadband seismometers for regional-scale induced seismicity monitoring; (2) To quantify the practical low-frequency limit of geophones after instrument response correction; (3) To assess the maximum event magnitude that can be accurately analyzed using geophone data.

Field experiment setup
A seismic station, S8.MB01, was deployed adjacent to TexNet station TX.MB12 (Figure 1) in 2023 to evaluate the performance of an industry-standard geophone and a MEMS accelerometer for regional-scale induced seismicity monitoring. Data from both stations are publicly available through the IRIS Data Management Center (IRIS DMC). Station TX.MB12 is equipped with a broadband seismometer and an accelerometer. Station S8.MB01

contains a standard 3-component 5 Hz geophone, a low noise 3-component MEMS accelerometer, and a 3-component MEMS magnetometer. The geophone 3-component data are automatically transformed into the North-East-Down coordinates using orientations determined from magnetometer and accelerometer measurements. The geophone response is then calibrated with the MEMS accelerometer data, and the instrument response is subsequently removed. This preprocessing step is performed automatically in the cloud before the S8.MB01 data stream is transmitted to the IRIS DMC. In this study, we compare seismic events recorded by the two stations during 2025, with the instrument response also removed from the TX.MB12 data for consistency.

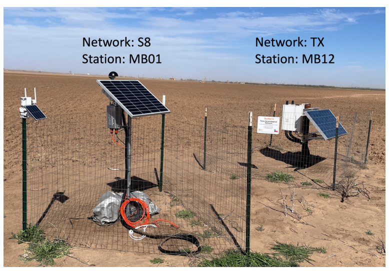

Figure 1: Photo of stations S8.MB01 and TX.MB12.

Comparisons of events within 30km

Within a 30 km radius of the two stations, a total of 448 seismic events with magnitudes ranging from M0.4 to M3.3 were recorded during 2025 (Figure 2a). P- and S-wave onsets were manually picked from the waveform data, and their corresponding signal-to-noise ratios (SNRs) were calculated. The P-wave SNR is defined as the ratio of the standard deviations of the vertical-component data in one-second windows following and preceding the onset time. The S-wave SNR is computed as the root-mean-square (RMS) of the SNRs from the two horizontal components. Figure 3a shows the distribution of P- and S-wave SNRs for events recorded by TX.MB12. Among the 448 events, 236 exhibit P- and S-wave phases that are difficult to identify due to low SNR. Figure 3b presents the cross-correlation coefficients between waveforms recorded by TX.MB12 and S8.MB01. Correlation coefficients exceed 0.85 for data with SNR > 2, indicating strong waveform consistency between the geophone and broadband seismometer. Examples of events with high and low SNRs are shown in Figure 4. Waveforms from TX.MB12 (blue) and S8.MB01 (black) are nearly identical, with minor discrepancies primarily attributed to high-frequency background noise. For events with well-defined S-wave arrivals, source parameters were estimated using Brune's source model (Brune, 1970) based on the two horizontal components. Local site effects were accounted for using the rock–soil mixed site model of Boore and Joyner (1997). Geometrical spreading was corrected using the reported event locations, and a constant quality factor (Q) of 300 was applied to compensate for attenuation. Comparisons of seismic moment and corner frequency derived from TX.MB12 and S8.MB01 data (Figure 5) show differences within about 10%, which can largely be attributed to the influence of high-frequency surface noise.

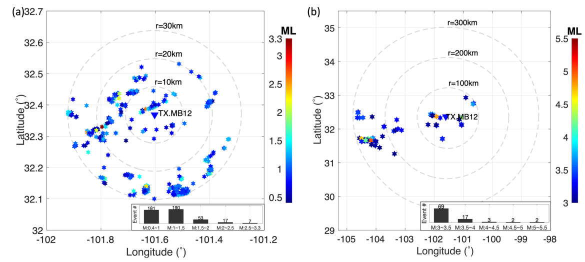

Figure 2: Event distributions: (a) within 30 km and (b) magnitude ≥ 3.

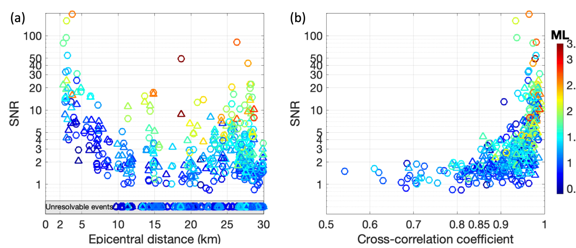

Figure 3: (a) Variations in P-wave (circles) and S-wave (triangles) SNRs for events within a 30 km radius. (b) Cross-correlation coefficients of P-waves (circles) and S-waves (triangles) recorded by stations TX.MB12 and S8.MB01 for events with resolvable phases. The gray-shaded region in (a) represents events for which P- or S-wave phases are unresolvable, and SNR values are therefore not computed.

Comparisons of events with magnitudes ≥ M3.0

During 2025, 93 earthquakes with magnitudes ≥ M3.0 occurred within 300 km of the two stations (Figure 2b). The largest event, with a magnitude of M5.4, occurred near Pecos, Texas, approximately 281 km away. Because S-waves at such distances are strongly affected by surface waves, only P-wave data are analyzed in this section. The SNRs and cross-correlation coefficients, as shown in Figure 6, were computed using the same approach as in the previous section, except that the time window for SNR calculation was extended to 2 s to accommodate the longer signal duration at greater distances. Among these events, 24 had unresolvable phases due to poor SNR. For the remaining events, P-wave cross-correlation coefficients exceed 0.9 for data with SNR > 2. Compared to the <30 km dataset, the agreement between TX.MB12 and S8.MB01 waveforms is even higher for larger events, likely due to their lower frequency content, which is less susceptible to high-frequency surface noise.

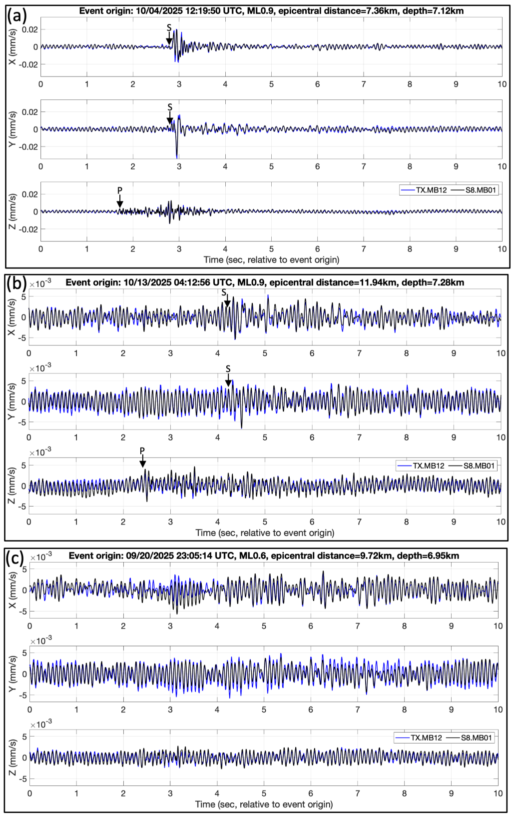

Figure 4: Example event data illustrating cases with (a) high SNR (P-wave SNR = 2.47, S-wave SNR = 7.04), (b) low SNR (P-wave SNR = 1.25, S-wave SNR = 2.18), and (c) unresolvable P- and S-wave phases.

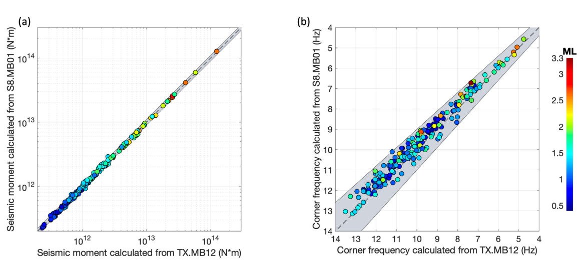

Figure 5: Comparison of seismic moment (a) and corner frequency (b) derived from S-wave waveforms of events recorded at TX.MB12 and S8.MB01. Gray-shaded areas indicate a ±10% deviation from the diagonal.

Figure 7 shows three-component waveform and amplitude-spectrum comparisons for the M5.4 event. The average cross-correlation coefficients (green dots) calculated from successive 1s time windows are 0.95, 0.98, and 0.93 for the three components over a 120s interval. The corresponding amplitude spectra show strong consistency between the two sensors down to approximately 0.2 Hz, confirming that the 5 Hz geophone can reliably record seismic data at frequencies as low as 0.2 Hz after response correction.

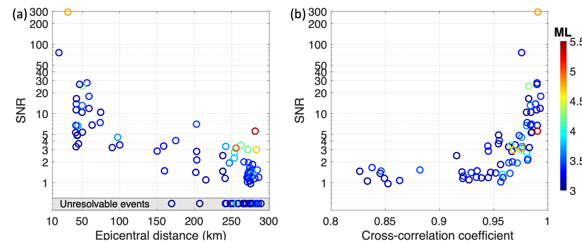

Figure 6: (a) Variations in P-wave SNRs for events with magnitudes>=3. (b) Cross-correlation coefficients of P-waves recorded by stations TX.MB12 and S8.MB01 for events with resolvable phases. The gray-shaded region in (a) represents events for which P-wave phases are unresolvable, and SNR values are therefore not computed.

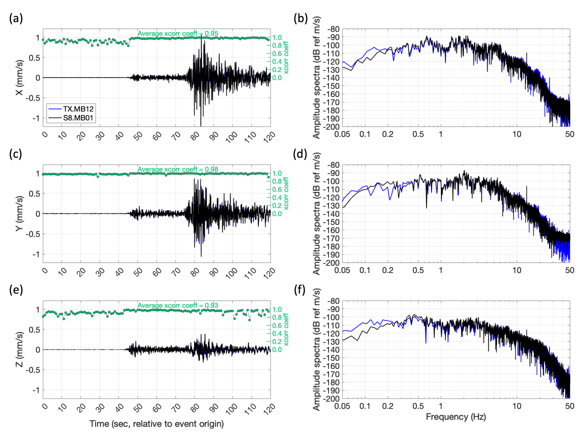

Figure 7: Comparison of three-component waveforms (left) and corresponding amplitude spectra (right) between TX.MB12 (blue) and S8.MB01 (black). Green dots in the waveform plots show cross-correlation coefficients calculated from successive 1s time segments of TX.MB12 and S8.MB01 data.

Noise and distance sensitivity analysis

As shown in Figure 8, the self-noise levels of a Nanometrics Trillium Compact seismometer and a 5 Hz geophone are nearly below the NLNM above 0.2 Hz. The geophone's self-noise is even lower than that of the seismometer above 2 Hz, which corresponds to the corner frequency of M3~M4 earthquakes. This indicates that the geophone is actually more sensitive than the seismometer for detecting small-to-moderate events that are critical for assessing the likelihood of exceeding regulatory alert thresholds. Below 2 Hz, although the geophone exhibits slightly higher self-noise than the seismometer, it remains below the NLNM down to about 0.2 Hz. In most environments, ambient background noise is significantly higher than the geophone's self-noise. Since only relatively large earthquakes (M4 and above) generate appreciable energy below 1 Hz within moderate distances (e.g., ~100 km), a 5 Hz geophone can still detect signals down to 0.1 Hz without difficulty. Therefore, for regional-scale monitoring (within ~100 km), a properly calibrated 5 Hz geophone can achieve detectability comparable to that of a broadband seismometer across the 0.1–50 Hz frequency range.

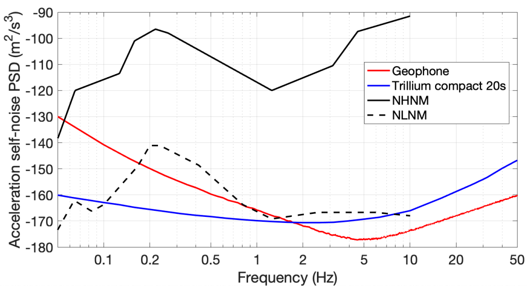

Figure 8: Comparison of the self-noise levels of a Nanometrics Trillium Compact seismometer (blue) and a 5Hz geophone (red). The sold and dashed black curves respectively represent the New High Noise Model (NHNM) and New Low Noise Model (NLNM).

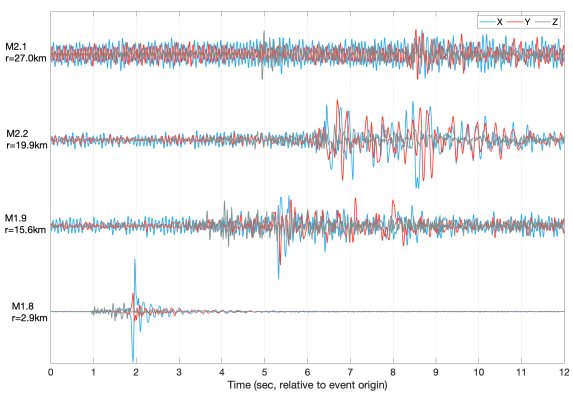

Figure 9: Examples of waveforms recorded at TX.MB12 for four events of similar magnitude occurring at different distances from the station.

Figure 9 shows three-component waveforms of four earthquakes with magnitudes around M2, located at different distances from the station. For the nearest event (2.9 km away), the P- and S-wave onsets are clearly identifiable, whereas at larger distances, both phases become increasingly dispersive, resulting in greater uncertainty in the picking of arrival times. Analysis of the full event dataset indicates that the station-to-event distance must generally be less than 10–15 km to obtain clear P- and S-wave arrivals for events of magnitude ≥ M1. Beyond this distance, the signals become dispersive and first-break picks carry higher uncertainty. Moreover, prior work by Fang et al. (2024) demonstrated that data recorded at large offsets exhibit reduced sensitivity to event depth.

As a practical guideline, a dense array with inter-station spacing of ≤10 km is required to reliably locate events with magnitudes ≥ M1, while smaller events demand even denser coverage. Under such conditions, cost-effective geophones are preferable to broadband seismometers for constructing dense monitoring arrays.

Conclusion

This study demonstrates that properly calibrated 5 Hz geophones can serve as an effective and economical alternative to broadband seismometers for regional-scale induced seismicity monitoring. The comparison between collocated sensors shows excellent waveform agreement, with cross-correlation coefficients exceeding 0.85 for events with magnitudes ranging from M0.4 to M3.3 within a 30km radius, and exceeding 0.9 for events with magnitudes of M3 and greater within a 300km distance, provided that the signal-to-noise ratio (SNR) is greater than 2. After instrument response removal, geophones accurately reproduce seismic signals down to approximately 0.2 Hz, covering the dominant frequency range of regional induced earthquakes, including those up to M5.4, the largest event analyzed in this study. Noise analysis further indicates that the self-noise level of a 5 Hz geophone is comparable to that of a broadband seismometer in the 0.2–50 Hz range, and its usable frequency range can likely extend to about 0.1 Hz for regional monitoring (within ~100 km). Therefore, with proper calibration and response correction, a 5 Hz geophone can achieve performance comparable to a broadband seismometer in both frequency response and noise characteristics for frequencies above 0.1 Hz. Given their low cost, durability, and ease of deployment, industry-grade geophones are particularly advantageous for establishing dense seismic arrays, offering a practical and scalable solution for improving event location accuracy and source mechanism characterization in regional and local induced seismicity monitoring.

Acknowledgments

We would like to express our gratitude to HighPeak Energy Inc., SM Energy, and Birch Resources for the great support in this study.